SCIENCE CHINA
Chemistry

•ARTICLES•

May 2024 Vol.67 No.5: 1664–1671
https://doi.org/10.1007/s11426-023-1953-2

In-situ construction of PDOL electrolyte with dual-reinforced stable interface for high-voltage lithium metal batteries

Yingkang Wu[2,3†], Yuzhou Bai[3†], Wujie Dong[3], Xue Wang[3], Wenqin Ma[3*] & Fuqiang Huang[1*]

[1]*State Key Lab of Metal Matrix Composites, School of Materials Science and Engineering, Shanghai Jiao Tong University, Shanghai 200240, China;*
[2]*School of Physical Science and Technology, Shanghai Tech University, Shanghai 201210, China;*
[3]*Shanghai Institute of Ceramics, Chinese Academy of Sciences, Shanghai 200050, China*

Received December 2, 2023; accepted February 5, 2024; published online April 9, 2024

In-situ polymerized electrolytes significantly enhance the interfacial compatibility of lithium metal batteries (LMBs). Typically, *in-situ* polymerized 1,3-dioxolane (PDOL) exhibits low interfacial resistance, yet still suffers from low ionic conductivity and a narrow electrochemical stability window (ESW). Here, an ultra-stable PDOL-based polymer electrolyte is developed by incorporating plasticizers of tetramethylene sulfone (TMS) and fluorinated ethylene carbonate (FEC) into the 3D cross-linked network, achieving a significant enhancement in the transport capacity and efficiency of Li-ion. The ionic conductivity reaches 3.63×10^{-4} S cm^{-1} even at room temperature, and the transference number (t_{Li^+}) is even higher at 0.85. Furthermore, the ESW of this electrolyte can be increased to 4.5 V with the addition of TMS, which forms a thin and robust antioxidant cathode-electrolyte interface (CEI) on the surface of high-voltage $LiCoO_2$. FEC generates an inorganic-rich solid-electrolyte interface (SEI) on the Li anode, which effectively inhibits the growth of lithium dendrites. Benefiting from the aforementioned advantages, the high-voltage lithium metal battery demonstrates outstanding long-cycle stability, with 93.2% capacity retention after 200 cycles. This work offers a straightforward and accessible method for the practical implementation of high energy density *in-situ* polymerized solid-state LMBs.

solid polymer electrolyte, *in-situ* polymerization, PDOL, high-voltage LMBs

Citation: Wu Y, Bai Y, Dong W, Wang X, Ma W, Huang F. *In-situ* construction of PDOL electrolyte with dual-reinforced stable interface for high-voltage lithium metal batteries. *Sci China Chem*, 2024, 67: 1664–1671, https://doi.org/10.1007/s11426-023-1953-2

1 Introduction

Rapid market expansion of electronics and electric vehicles is driving the development of higher energy density and safer flexible electronic devices [1–5]. Routine liquid lithium-ion batteries (LIBs) have been widely used in electric power systems. However, there are serious problems with conventional organic liquid electrolytes, such as leakage, volatility, and flammability, which pose a safety risk to flexible LIBs, particularly in high-temperature conditions [6]. Replacing organic liquid electrolytes with solid polymer electrolytes (SPEs) can alleviate the safety concerns of LIBs and provide better processability for electronic devices [7,8]. Unfortunately, the complex ex-situ synthesis methods of SPEs result in poor contact and affinity at the electrolyte/electrode interface [9,10].

Recently, *in-situ* polymerization strategies for SPEs have received much attention [11–13]. The *in-situ* polymerization strategy typically involves injecting a low-viscosity precursor into the battery, followed by free radical polymerization or ring-opening polymerization of monomers using an initiator. As a result, the *in-situ* polymerization process can fill all the gaps/voids of the electrodes, thus

†These authors contributed equally to this work.
*Corresponding authors (email: huangfq@sjtu.edu.cn; mawenqin@mail.sic.ac.cn)

© Science China Press 2024

achieving a tight interfacial contact between the SPEs and the electrodes. Up to now, several SPEs synthesized by *in-situ* polymerization methods have been widely reported. These include poly(vinylidene carbonate) (PVC) [14–16], poly(trimethylpropane triacrylate) (ETPTA) [17–20], poly (ethylene glycol diacrylate) (PEGDA) [21–23], poly(vinyl ethylene carbonate) (PVEC) [24,25], poly(tetrahydrofuran) (PTHF) [26,27] and poly(1,3-dioxolane) (PDOL) [28–36].

1,3-Dioxolane (DOL) is susceptible to Lewis acid-initiated ring-opening polymerization and is one of the most commonly used monomers for *in-situ* polymerization. Archer *et al*. reported the *in-situ* curing of PDOL electrolytes initiated with low concentrations of $Al(OTf)_3$ [29], and the *in-situ* curing of SPEs efficiently overcame the problem of high interfacial resistances. Guo *et al*. initiated the generation of quasi-solid SPEs from DOL/DME liquid electrolytes using $LiPF_6$ [28]. However, similar to other polyether electrolytes, the room-temperature (RT) ionic conductivity of PDOL electrolytes is only about 10^{-6} S cm^{-1}, which hinders their application in practical situations [8]. In addition, the polyether electrolyte exhibits poor oxidative stability [37–40] and undergoes significant decomposition when in contact with cathode materials (such as $LiCoO_2$) under high voltage conditions (>4.2 V). This decomposition ultimately results in a decline in battery performance.

In this study, an *in-situ* polymerized electrolyte with dual-reinforced stable interface is synthesized by incorporating high boiling point and safety plasticizers, tetramethylene sulfone (TMS), and fluorinated ethylene carbonate (FEC) into the 3D PDOL cross-linked network. The addition of plasticizers can disrupt the crystalline chain segments of PDOL and increase the ionic conductivity of the electrolyte. In addition, the introduction of TMS can form a thin and stable cathode-electrolyte interface (CEI) layer on the surface of $LiCoO_2$, which enhances the compatibility of the electrolyte with the high-voltage $LiCoO_2$. The introduction of FEC further generates an inorganic-rich solid electrolyte interface layer (SEI) on the surface of Li, effectively inhibiting the growth of lithium dendrites. The electrolyte possesses a high ionic conductivity at RT (3.63×10^{-4} S cm^{-1}), excellent oxidative stability (4.5 V), and a high Li-ion transference number (t_{Li^+} = 0.85). Benefiting from the aforementioned advantages, the Li/$LiCoO_2$ battery exhibits exceptional long cycle stability at 4.3 V, with 93.2% capacity retention after 200 cycles.

2 Results and discussion

2.1 Electrolyte preparation and characterization

The preparation of TMS/FEC-modified PDOL-based *in-situ* polymerized electrolytes is shown in detail in Figure 1. $LiBF_4$ is used as an initiator for the ring-opening polymerization of DOL. Trimethylolpropane triglycidyl ether (TTE) is a cross-linking agent that contains ethylene oxide groups. The addition of a small amount of TTE leads to a 3D PDOL cross-linked structure. This structure enhances the mechanical strength and solvent absorption capacity of PDOL, allowing for the complete encapsulation of TMS and FEC within the 3D polymer network. The *in-situ* polymerization mechanism is cationic ring-opening polymerization (Figure 1). $LiBF_4$ in the precursor solution can spontaneously decompose into LiF and the Lewis acid BF_3 at RT. BF_3 is then protonated by reacting with trace water in the precursor solution and triggers the cationic ring-opening polymerization of DOL monomer and TTE [31].

The original PDOL electrolyte and the electrolytes introduced with different plasticizers are named PDOL, PDOL-T, and PDOL-T-F, respectively. All three types of electrolytes are left to cure at RT for 72 h. Based on the optical photographs of PDOL-T-F before and after polymerization (Figure 2a,b), it is evident that there is no liquid

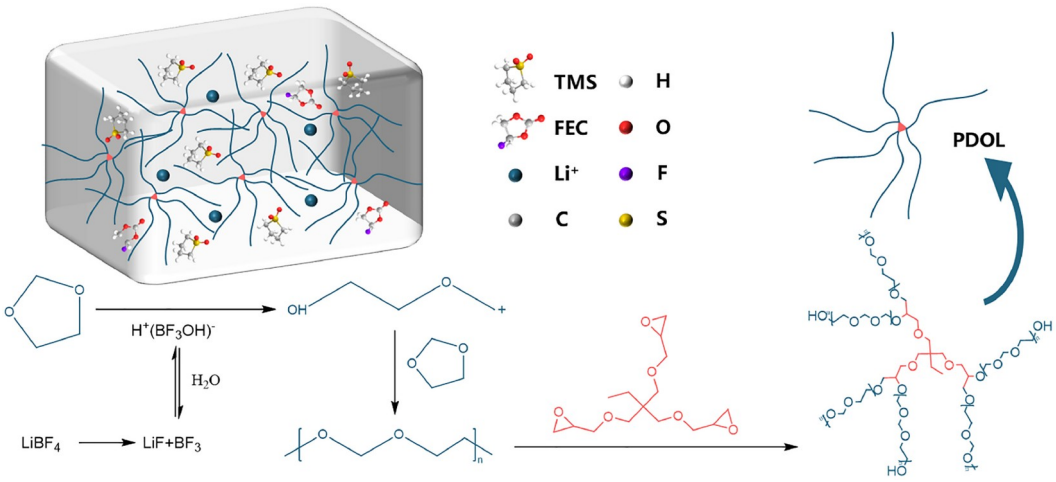

Figure 1 Preparation and mechanism of *in-situ* plasticized PDOL electrolyte with 3D cross-linked network induced by $LiBF_4$ (color online).

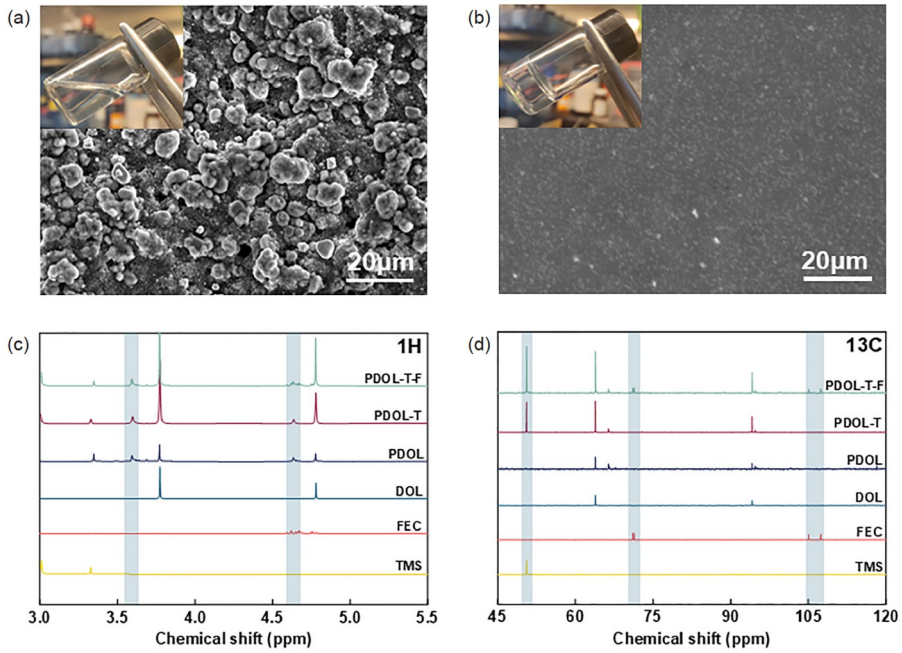

Figure 2 Digital photo of precursor solutions and SEM image of the $LiCoO_2$ electrode (a) before and (b) after *in-situ* polymerization. (c) ^{1}H NMR spectra and (d) ^{13}C NMR spectra of the precursor solution components and the *in-situ* polymerized electrolyte (color online).

flow in the glass bottle after curing. When the liquid precursor is injected into the battery, it can easily wet the separator and penetrate into the voids of the $LiCoO_2$ particles, which significantly reduces the interfacial impedance and improves the interfacial compatibility (Figure S2, Supporting Information online). As can be seen from the scanning electron microscope (SEM) images (Figure 2b), $LiCoO_2$ particles are completely infiltrated by the precursor, and a uniform film of a 3D PDOL cross-linked network is generated on the surface of $LiCoO_2$ after 72 h of standing.

The structure of the electrolyte is characterized using nuclear magnetic resonance (NMR) 1H and 13C spectra. In the 1H NMR spectra (Figure 2c), the peaks observed at 3.59 ppm and 4.63 ppm for PDOL and PDOL-T-F correspond to the –O–CH_2–O– and –CH_2–O–CH_2– chains, respectively. Compared to PDOL, the peaks observed at 50.33 ppm in the 13C NMR spectrum of PDOL-T-F (Figure 2d) are attributed to TMS, whereas the peaks at 71.15 ppm, 105.06 ppm, and 107.28 ppm correspond to FEC. The results successfully demonstrate the generation of the polymer network of PDOL and the introduction of TMS and FEC.

2.2 Characterization and electrochemical performance of electrolytes

The oxidative stability of the electrolyte is evaluated based on the electrochemical stability window (ESW). A wider ESW can better match high-voltage cathode materials, thereby improving the energy density of the battery. Linear scanning voltammetry (LSV) testing is performed by assembling a coin cell with Li and stainless steel (SS) (Figure 3a). The ESW of PDOL is 4.3 V, which is higher than the value reported in the literature (4.1 V) [30]. This difference may be attributed to the presence of a small percentage of TTE, which promotes the conversion of the DOL monomer to PDOL. As a result, the oxidative decomposition of the DOL monomer is reduced [32]. By adding TMS plasticizer, the ESW can be increased to 4.5 V. It is mainly attributed to the low energy level of highest occupied molecular orbital (HOMO) of TMS [41]. For PDOL-T-F, the ESW is 4.5 V, indicating that the introduction of FEC does not influence the oxidative stability of the electrolyte. The addition of plasticizers achieves compatibility between the electrolyte and the high-voltage cathode.

Ionic conductivity is a crucial performance parameter for SPEs. In general, the RT ionic conductivity of SPEs needs to be greater than 10^{-4} S cm^{-1} in order to ensure the proper functioning of the battery [8]. The ionic conductivities of the three types of electrolytes are evaluated using electrochemical impedance spectroscopy (EIS) of SS/SS symmetric cells at 30 °C (Figure 3b). The RT ionic conductivity of PDOL is only 5.08×10^{-6} S cm^{-1}, indicating that the cell is challenging to operate effectively at RT. In comparison, PDOL-T-F has the highest ionic conductivity at RT with a value of 3.63×10^{-4} S cm^{-1}. The Arrhenius curve describes the relationship between temperature and ionic conductivity (Figure S1 and Figure 3c), followed by further calculations of the ionic activation energy (E_a) of the SPEs. The calculated values for PDOL, PDOL-T, and PDOL-T-F are 0.355,0.088, and 0.071 eV, respectively. Therefore, the ionic conductivity

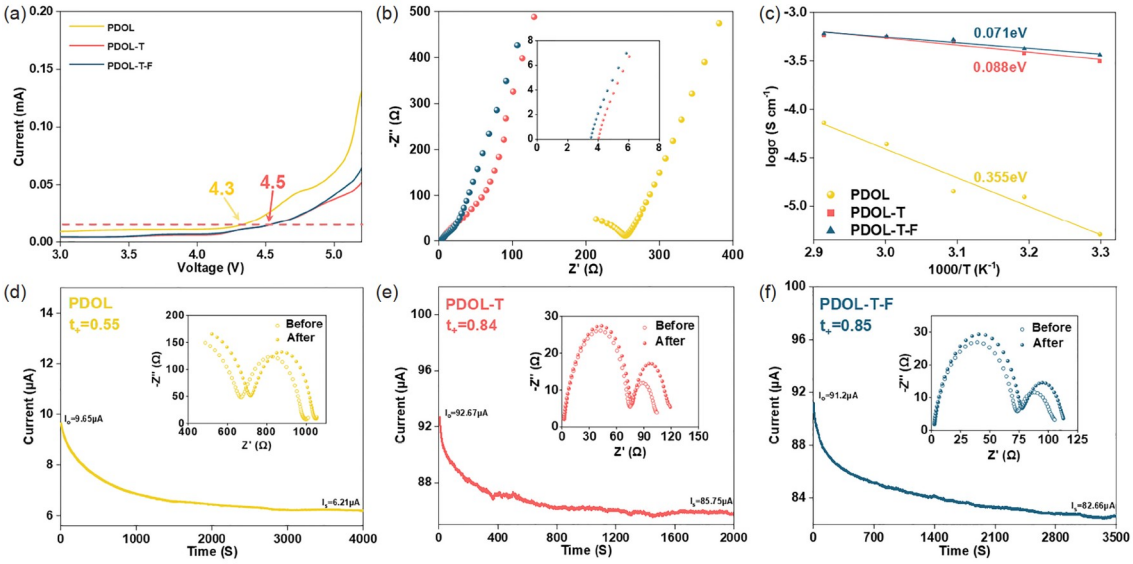

Figure 3 (a) LSV curves of various *in-situ* polymerization samples. (b) The EIS curves of SS/SS symmetric cells at RT (30 °C). (c) Temperature dependence of Li-ion conductivity in *in-situ* polymerization electrolytes. (d–f) Steady-state polarization curves of Li/Li symmetric cells assembled with various electrolytes (inset: EIS curves before and after polarization) (color online).

of PDOL-T-F exhibits minimal temperature dependence.

t_{Li^+} is a crucial parameter for evaluating the efficiency of Li-ion transport. High t_{Li^+} can effectively reduce concentration polarization and the growth of lithium dendrites during charge/discharge. This leads to uniform deposition/stripping behavior of Li and ultimately improves battery cycle stability [42]. The t_{Li^+} is measured by using the steady-state polarization curves of Li/Li symmetric cells (Figure 3d–f). The t_{Li^+} of PDOL-T-F (0.85) is higher than that of PDOL (0.55) and PDOL-T (0.84), which promotes faster charge/discharge rates and longer battery cycle life.

2.3 Performances of solid-state lithium battery

Figure 4a demonstrates the cycling performance of Li/Li-CoO_2 batteries assembled with different electrolytes. The charging cutoff voltage is fixed at 4.3 V, and the temperature is at RT (60 °C for PDOL battery). Batteries are initially activated at a rate of 0.2 C for the first two cycles and then operated at 1 C for the subsequent cycles. Due to the low ionic conductivity and narrow ESW of the PDOL, the initial discharge specific capacity of the PDOL battery is 95.6 mAh g^{-1}, and only 23 mAh g^{-1} is retained after 100 cycles. The initial specific capacity of the PDOL-T battery can be up to 145.2 mAh g^{-1}. Unfortunately, the specific capacity decays even faster. The capacity retention after 50 cycles of the battery is only 12.5%. This may be attributed to the fact that TMS reacts violently with lithium metal during battery operation [43]. The deposition/stripping behavior of Li is unstable, ultimately resulting in significant capacity degradation of the battery. It can also be verified by the low average coulombic efficiency of the PDOL-T battery (Figure 4b). For the PDOL-T-F battery, FEC contributes to the formation of a stable SEI. It realizes the highest initial specific capacity of 146.7 mAh g^{-1} and a capacity retention of 93.2% after 200 cycles. TMS and FEC enable the Li/PDOL-T-F/$LiCoO_2$ battery to achieve a combination of high oxidative stability and long cycle life. In order to demonstrate the universality of PDOL-T-F when paired with high-voltage cathodes, a Li/PDOL-T-F/$Li_2Ni_{0.8}Co_{0.1}Mn_{0.1}O_2$ battery is assembled for validation (Figure S3). The battery still maintains a high capacity retention rate of 86.3% after 300 cycles.

The charge/discharge voltage curves of the Li/$LiCoO_2$ batteries are shown in Figure 4d–f**.** The polarization voltages of the PDOL and PDOL-T batteries increase rapidly as the batteries begin to run, while the polarization voltage of the PDOL-T-F battery remains almost constant during the 1st and 200th cycles, which can be attributed to the high t_{Li^+} in the PDOL-T-F. The rapid charge/discharge performance of the battery is also affected by t_{Li^+}. The Figure 4c shows the rate capacity of batteries assembled with different electrolytes. It is evident that at 3C, the PDOL-T-F battery exhibits the highest discharge specific capacity (113 mAh g^{-1}), which is consistent with the performance of t_{Li^+}.

To further investigate the effect of different electrolytes on Li deposition/stripping behavior, Li/Li symmetric cells are assembled for cycling tests (Figure 4g). The current density and specific capacity are fixed at 0.2 mA cm^{-2} and 0.2 mAh cm^{-2}, and the temperature is at RT (60 °C for PDOL cell). The polarization voltage of the PDOL cell initially reaches 140 mV, and after 100 h of operation, it increases to about 230 mV and continues to rise gradually. After the addition of TMS, the initial polarization voltage is increased to 600mV,

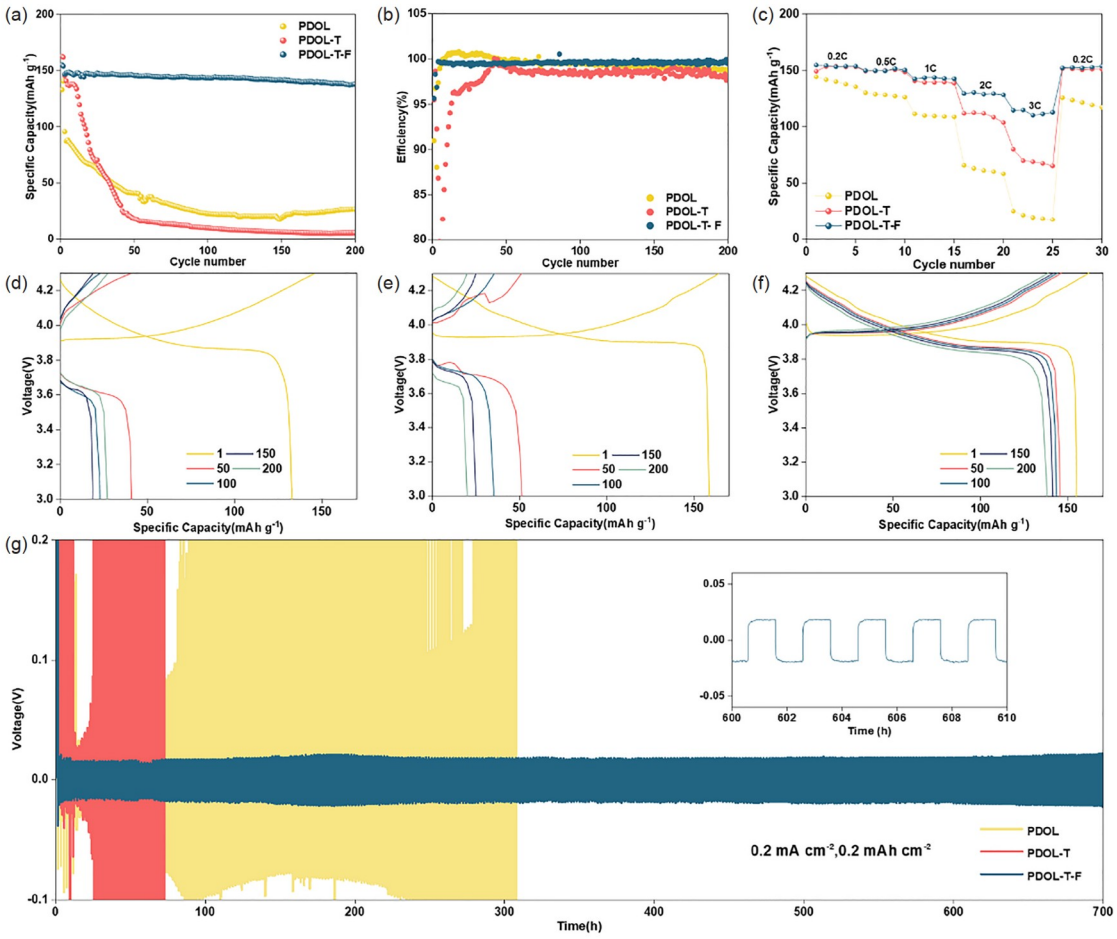

Figure 4 (a) Cycling performance, (b) coulomb efficiency and (c) rate capability of Li/$LiCoO_2$ batteries with PDOL, PDOL-T and PDOL-T-F at 4.3V. (d–f) The charge/discharge voltage curve of Li/$LiCoO_2$ batteries during 200 cycles (from left to right: PDOL, PDOL-T, and PDOL-T-F). (g) Plating and stripping behaviors of Li symmetric cells with various electrolytes at a current density of 0.2 mA cm^{-2} and a specific capacity of 0.2 mAh cm^{-2} (PDOL is tested under 60 °C, other electrolytes are tested at RT) (color online).

which exceeds 1V after 50 h and causes a short circuit. After adding FEC, the initial polarization voltage of the battery is only about 16 mV. With the increase in cycle time, the polarization voltage essentially stabilizes and remains at only 20mV after 700 h. Changing the current density and specific capacity to 0.1 mA cm^{-2} and 0.1 mAh cm^{-2} (Figure S4), the polarization voltage of the PDOL-T-F cell cycling for 1800 h is even lower at 11 mV, which is significantly better than that of the PDOL and PDOL-T. Even at a high current density of 1 mA cm^{-2} (Figure S5), the Li/PDOL-T-F/Li cell can maintain stable operation for 160 h. Thanks to the excellent ionic conductivity and t_{Li^+}, the Li/PDOL-T-F/Li cell exhibits excellent Li deposition/stripping stability and inhibition of lithium dendrite growth.

2.4 Characterization of CEI and Li surface

In order to investigate the factors responsible for the stable cycling of PDOL-T-F battery at high voltage, Li/$LiCoO_2$ batteries are disassembled after 200 cycles using three different electrolytes. Subsequently, morphological observations and elemental analyses are conducted on the surface of $LiCoO_2$ particles. SEM images (Figure S6,S7) of LiCoO2 particles after cycling of the three electrolytes are not significantly different. The CEI of the $LiCoO_2$ surface is determined using transmission electron microscopy (TEM) (Figure 5a). We can clearly observe that the $LiCoO_2$ electrode develops an uneven thickness of the CEI layer after cycling in PDOL. The thickest CEI layer reaches 40 nm, which significantly impedes the transport of Li-ions at the interface. Moreover, a partial surface of $LiCoO_2$ receives no CEI, which means that the electrolyte is not protected from oxidative decomposition under high-voltage conditions. For both PDOL-T and PDOL-T-F, a thin and uniform layer of CEI can be formed on the surface of $LiCoO_2$, which effectively prevents the decomposition of the electrolyte at the cathode side.

X-ray photoelectron spectroscopy (XPS) is chosen to further analyze the elemental composition of CEI. From the O 1s spectra (Figure 5b), it can be observed that the C–O

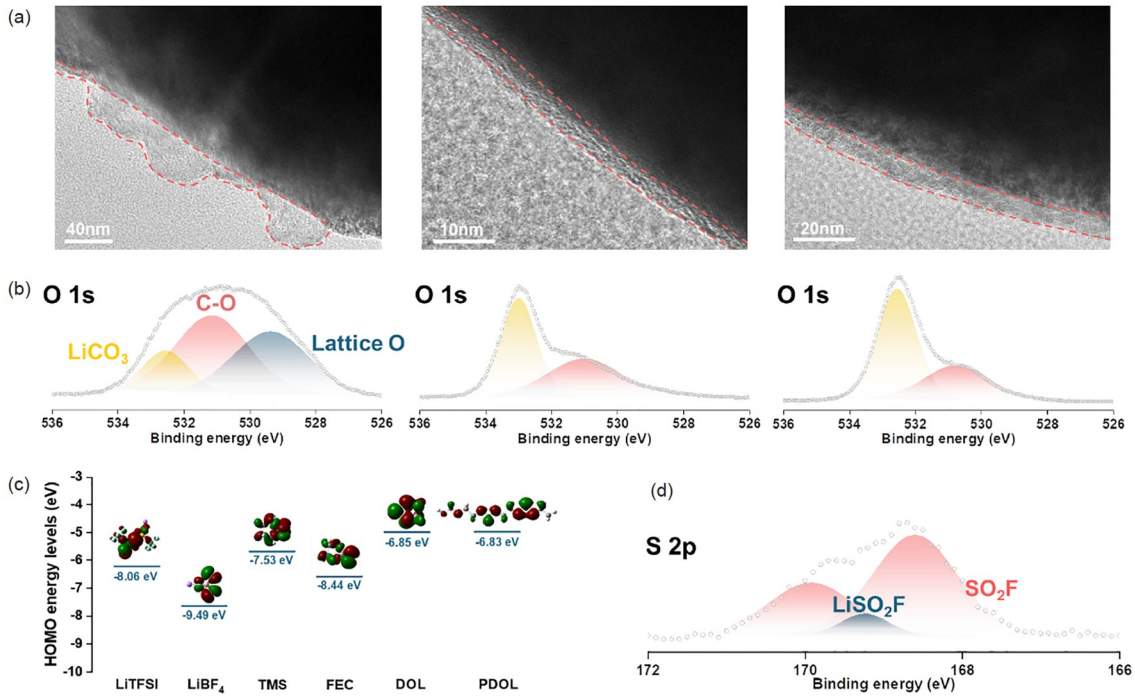

Figure 5 (a) CEI images and (b) O 1s XPS images of $LiCoO_2$ cathodes disassembled from Li/$LiCoO_2$ batteries after 200 cycles (from left to right: PDOL, PDOL-T, and PDOL-T-F). (c) HOMO levels of LiTFSI, $LiBF_4$, TMS, FEC, DOL, and PDOL. (d) S 2p XPS images of $LiCoO_2$ cathodes disassembled from Li/$LiCoO_2$ batteries with PDOL-T-F after 200 cycles (color online).

signals on the $LiCoO_2$ surface of PDOL battery after cycling are more pronounced compared to PDOL-T and PDOL-T-F. It is speculated that the continuous decomposition of the electrolyte on the cathode surface generates more organic species. Furthermore, signals of lattice oxygen are observed, which again suggest the absence of CEI formation on parts of the $LiCoO_2$ surface. LiF and Li_3N are observed in the F 1s spectra (Figure S8) and N 1s spectra (Figure S9) of the $LiCoO_2$ after cycling in PDOL-T-F, which results from the decomposition of LiTFSI [44]. In addition, the more polar $LiSO_2F$ and SO_2F components [41] also appear in the S 2p spectra (Figure 5d), which effectively reduces the interfacial impedance and enables rapid conduction of Li-ion.

Figure 5c displays the highest occupied molecular orbital (HOMO) energies of commonly used battery materials obtained by quantum chemical calculations. The high HOMO values of both DOL (−6.85 eV) and PDOL (−6.83 eV) indicate that oxidative decomposition occurs at high voltages. PDOL electrolytes can generate a fragile layer of CEI on the surface of $LiCoO_2$. However, the degradation of PDOL on the cathode side cannot be effectively prevented. Both TMS (−7.53 eV) and FEC (−8.44 eV) have lower HOMO energies than PDOL, which further enhances the ESW of the electrolyte. Moreover, due to the higher adsorption energy of TMS with the cathode material, it can preferentially form a stable CEI on the cathode surface [41].

Finally, Li/Li symmetric cells cycled for 500 h with different electrolytes are disassembled, and the Li metal surface is characterized using SEM and XPS. From the SEM images of the Li surface cycled in PDOL (Figure 6a), we can clearly observe numerous irregular lithium dendrites, which can lead to battery failure. For PDOL-T, after cycling, Li anode not only generates lithium dendrites but also a significant amount of dead lithium and cracks. The PDOL-T-F exhibits excellent stability and resistance to lithium dendrite growth. The Li cycled in PDOL-T-F has the cleanest and glossiest surface. It also exhibits a compact and dendrite-free Li deposition layer, which can be observed from its SEM image and consists of chunky metallic Li. For the demand of lithium metal anode, achieving a more uniform and compact lithium deposition is crucial for better cycle performance. This requirement is also supported by the actual test results of batteries with PDOL-T-F. There are two main factors contributing to the superior lithium compatibility of PDOL-T-F. Firstly, it has the highest RT ionic conductivity and t_{Li^+}, which promotes uniform lithium deposition. Secondly, the addition of FEC enhances the stability of the electrolyte on the Li anode. This reduces the negative effects of electrolyte decomposition on ion-transport performance and minimizes the impact of decomposition by-products on lithium deposition.

The elemental composition of the Li surface is tested using XPS. The results of the F 1s spectrum (Figure 6b) and N 1s spectrum (Figure S10) show that the Li surface after PDOL

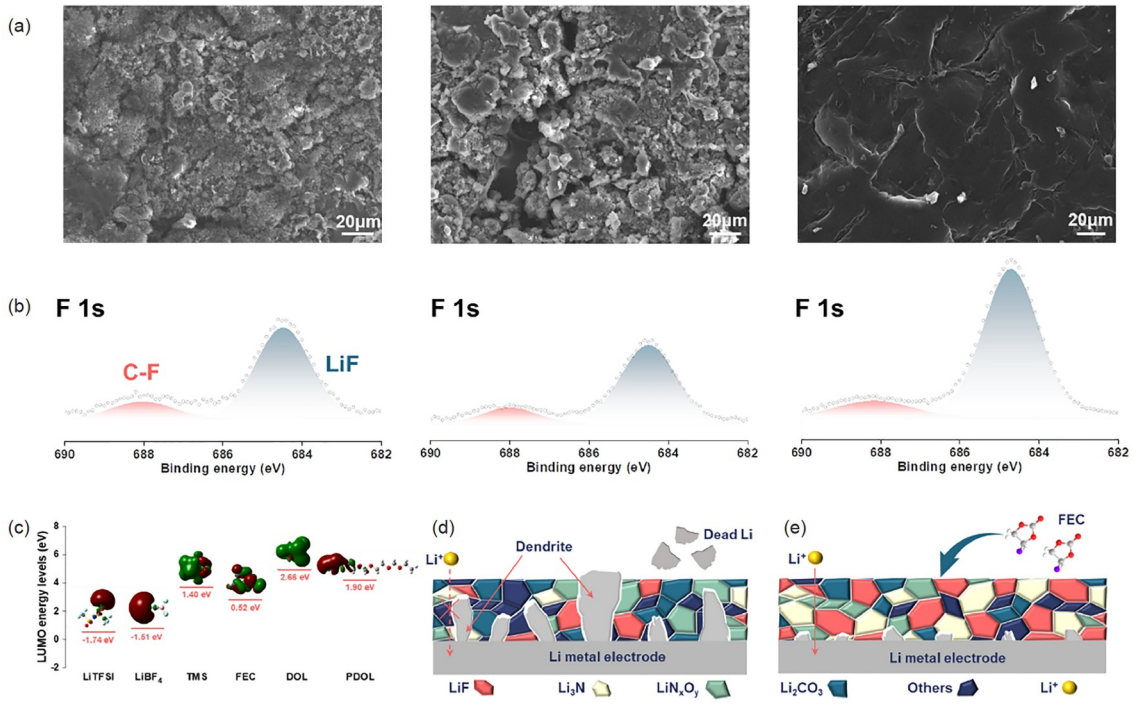

Figure 6 (a) SEM images and (b) F 1s XPS images of Li surface disassembled from Li/Li symmetric cells after 500 h (from left to right: PDOL, PDOL-T, and PDOL-T-F). (c) LUMO levels of LiTFSI, $LiBF_4$, TMS, FEC, DOL, and PDOL. Schematic diagram of SEI in (d) PDOL, PDOL-T, and (e) PDOL-T-F (color online).

cycling contained the lowest amount of LiF and Li_3N, which mainly originated from the decomposition of LiTFSI [44]. The signals of LiF and Li_3N are significantly enhanced after the introduction of TMS and FEC. In addition to the two components, the generation of Li_2CO_3 and other organic species (Figure S11) occurs as a result of the reduction of organic solvents [45]. Previous studies [46–48] have shown that the inorganic components (LiF, Li_3N, Li_2CO_3, *etc.*) tend to exhibit better comprehensive performance compared to the organic components in SEI. LiF possesses excellent electronic insulating properties, high surface energy, and mechanical strength, while Li_3N exhibits excellent ionic conductivity in the room temperature [46]. Compared with the SEI in PDOL (Figure 6d), the inorganic-rich SEI in PDOL-T-F (Figure 6e) can effectively promote the uniform deposition of lithium and inhibit the growth of lithium dendrites.

LiTFSI and $LiBF_4$ can selectively react with lithium metal to produce a SEI due to their low LUMO energy levels (Figure 6c). However, this SEI layer is relatively delicate and incapable of effectively preventing the continuous decomposition of TMS on the Li surface, resulting in the faster capacity degradation of the PDOL-T battery. Since the LUMO energy level of FEC is lower than that of TMS and the adsorption energy with lithium metal is stronger, an inorganic (LiF, Li_3N, *etc.*)-rich SEI is formed on the Li surface, which realizes the stable lithium deposition/stripping.

3 Conclusions

In summary, an *in-situ* polymerized electrolyte with dual-reinforced stable interface is synthesized by incorporating high boiling point and safety plasticizers, tetramethylene sulfone (TMS), and fluorinated ethylene carbonate (FEC) into the 3D PDOL cross-linked network. Compared to the original PDOL electrolyte, the PDOL-T-F assembled Li/$LiCoO_2$ battery achieves stable long cycling at 4.3 V. The excellent performance of the Li/PDOL-T-F/$LiCoO_2$ battery can be attributed to the following factors: (1) The introduction of the plasticizer disrupts the crystallinity of the polymer molecular chain and facilitates the dissociation of the lithium salts, greatly improving the Li-ion transport capacity and efficiency (RT ionic conductivity is 3.63×10^{-4} S cm^{-1}, t_{Li^+} = 0.85). (2) By adding TMS, the ESW can be increased from the original 4.3 V to 4.5 V, demonstrating remarkable oxidative stability. A thin and tough CEI is formed on the $LiCoO_2$ surface, which enhances compatibility with the high-voltage cathode. (3) Furthermore, by introducing FEC, PDOL-T-F can generate an inorganic-rich SEI on the surface of Li, effectively preventing the growth of lithium dendrites and promoting uniform deposition and stripping of Li. Based on the aforementioned advantages, the Li/PDOL-T-F/$LiCoO_2$ battery demonstrates exceptional long cycle stability at 4.3 V, with a capacity retention of 93.2% after 200 cycles. This work offers a straightforward and accessible method for

the practical implementation of high-voltage *in-situ* polymerized solid-state LMBs.

Acknowledgements This work was supported by the National Natural Science Foundation of China (52202327), and Science and Technology Commission of Shanghai Municipality (22ZR1471300).

Conflict of interest The authors declare no conflict of interest.

Supporting information The supporting information is available online at chem.scichina.com and link.springer.com/journal/11426. The supporting materials are published as submitted, without typesetting or editing. The responsibility for scientific accuracy and content remains entirely with the authors.

1 Chang J, Huang Q, Zheng Z. *Joule*, 2020, 4: 1346–1349
2 Zeng W, Shu L, Li Q, Chen S, Wang F, Tao XM. *Adv Mater*, 2014, 26: 5310–5336
3 Yang Y, Cui T, Li D, Ji S, Chen Z, Shao W, Liu H, Ren TL. *Nano-Micro Lett*, 2022, 14: 161
4 Hui Z, Zhang L, Ren G, Sun G, Yu HD, Huang W. *Adv Mater*, 2023, 35: 2211202
5 Zhang B-, Ren L, Wang Y-, Xu X, Du Y, Dou S-. *Interdisciplinary Mater*, 2022, 1: 354–372
6 Li M, Lu J, Chen Z, Amine K. *Adv Mater*, 2018, 30: 1800561
7 Lennartz P, Paren BA, Herzog-Arbeitman A, Chen XC, Johnson JA, Winter M, Shao-Horn Y, Brunklaus G. *Joule*, 2023, 7: 1471–1495
8 Zhou D, Shanmukaraj D, Tkacheva A, Armand M, Wang G. *Chem*, 2019, 5: 2326–2352
9 Ding P, Lin Z, Guo X, Wu L, Wang Y, Guo H, Li L, Yu H. *Mater Today*, 2021, 51: 449–474
10 Chen R, Li Q, Yu X, Chen L, Li H. *Chem Rev*, 2020, 120: 6820–6877
11 Cho YG, Hwang C, Cheong DS, Kim YS, Song HK. *Adv Mater*, 2019, 31: e1804909
12 Vijayakumar V, Anothumakkool B, Kurungot S, Winter M, Nair JR. *Energy Environ Sci*, 2021, 14: 2708–2788
13 Liu Q, Wang L. *Adv Energy Mater*, 2023, 13: 2301742
14 Tan SJ, Yue J, Tian YF, Ma Q, Wan J, Xiao Y, Zhang J, Yin YX, Wen R, Xin S, Guo YG. *Energy Storage Mater*, 2021, 39: 186–193
15 Zhang X, Gao G, Wang W, Wang J, Wang L, Liu T. *ACS Appl Mater Interfaces*, 2022, 14: 49811–49819
16 Zhang X, Zhang M, Wu J, Hu X, Fu B, Zhang Z, Luo B, Khan K, Fang Z, Xu Z, Wu M. *Nano Energy*, 2023, 115: 108700
17 Wen P, Lu P, Shi X, Yao Y, Shi H, Liu H, Yu Y, Wu ZS. *Adv Energy Mater*, 2020, 11: 2002930
18 Chen Z, Yang Y, Su Q, Huang S, Song D, Ma R, Zhu C, Lv G, Li C. *ACS Appl Mater Interfaces*, 2021, 13: 41946–41955
19 Wang A, Geng S, Zhao Z, Hu Z, Luo J. *Adv Funct Mater*, 2022, 32: 2201861
20 Bao C, Zheng C, Wu M, Zhang Y, Jin J, Chen H, Wen Z. *Adv Energy Mater*, 2023, 13: 2204028
21 Yu X, Liu Y, Goodenough JB, Manthiram A. *ACS Appl Mater Interfaces*, 2021, 13: 30703–30711
22 Yuan B, Zhao B, Wang Q, Bai Y, Cheng Z, Cong Z, Lu Y, Ji F, Shen F, Wang PF, Han X. *Energy Storage Mater*, 2022, 47: 288–296
23 Shi L, Wang W, Wang C, Zhou Y, Feng Y, Jia T, Wang F, Min Z, Hu J, Xue Z. *J Energy Chem*, 2023, 79: 253–262
24 Rong Z, Sun Y, Zhao Q, Cheng F, Zhang W, Chen J. *Chem Eng J*, 2022, 437: 135329
25 Qin S, Yu Y, Zhang J, Ren Y, Sun C, Zhang S, Zhang L, Hu W, Yang H, Yang D. *Adv Energy Mater*, 2023, 13: 2301470
26 Huang S, Cui Z, Qiao L, Xu G, Zhang J, Tang K, Liu X, Wang Q, Zhou X, Zhang B, Cui G. *Electrochim Acta*, 2019, 299: 820–827
27 Liu Q, Tan J, Liu Z, Hu X, Yu J, Wang X, Wu J, Cai B, Wang Q, Fu Y, Liu H, Li B. *ACS Appl Mater Interfaces*, 2022, 14: 26612–26621
28 Liu FQ, Wang WP, Yin YX, Zhang SF, Shi JL, Wang L, Zhang XD, Zheng Y, Zhou JJ, Li L, Guo YG. *Sci Adv*, 2018, 4: 5383
29 Zhao Q, Liu X, Stalin S, Khan K, Archer LA. *Nat Energy*, 2019, 4: 365–373
30 Geng Z, Huang Y, Sun G, Chen R, Cao W, Zheng J, Li H. *Nano Energy*, 2022, 91: 106679
31 Wen S, Luo C, Wang Q, Wei Z, Zeng Y, Jiang Y, Zhang G, Xu H, Wang J, Wang C, Chang J, Deng Y. *Energy Storage Mater*, 2022, 47: 453–461
32 Yang H, Zhang B, Jing M, Shen X, Wang L, Xu H, Yan X, He X. *Adv Energy Mater*, 2022, 12: 2201762
33 Mi YQ, Deng W, He C, Eksik O, Zheng YP, Yao DK, Liu XB, Yin YH, Li YS, Xia BY, Wu ZP. *Angew Chem Int Ed*, 2023, 62: e202218621
34 Bai Y, Ma W, Dong W, Wu Y, Wang X, Huang F. *ACS Appl Mater Interfaces*, 2023, 15: 26834–26842
35 Zhao J, Li M, Su H, Liu Y, Bai P, Liu H, Ma L, Li W, Sun J, Xu Y. *Small Methods*, 2023, 7: e2300228
36 Zhu J, Zhang J, Zhao R, Zhao Y, Liu J, Xu N, Wan X, Li C, Ma Y, Zhang H, Chen Y. *Energy Storage Mater*, 2023, 57: 92–101
37 Cabañero Martínez MA, Boaretto N, Naylor AJ, Alcaide F, Salian GD, Palombarini F, Ayerbe E, Borras M, Casas-Cabanas M. *Adv Energy Mater*, 2022, 12: 2201264
38 Chen X, Li X, Luo L, He S, Chen J, Liu Y, Pan H, Song Y, Hu R. *Adv Energy Mater*, 2023, 13: 2301230
39 Huo S, Sheng L, Xue W, Wang L, Xu H, Zhang H, He X. *InfoMat*, 2023, 5: e12394
40 Wang G, Liang Y, Liu H, Wang C, Li D, Fan L-. *Interdisciplinary Mater*, 2022, 1: 434–444
41 Dong L, Liu Y, Chen D, Han Y, Ji Y, Liu J, Yuan B, Dong Y, Li Q, Zhou S, Zhong S, Liang Y, Yang M, Yang C, He W. *Energy Storage Mater*, 2022, 44: 527–536
42 Zhou P, Zhang X, Xiang Y, Liu K. *Nano Res*, 2022, 16: 8055–8071
43 Ren X, Chen S, Lee H, Mei D, Engelhard MH, Burton SD, Zhao W, Zheng J, Li Q, Ding MS, Schroeder M, Alvarado J, Xu K, Meng YS, Liu J, Zhang JG, Xu W. *Chem*, 2018, 4: 1877–1892
44 Chen D, Zhu M, Kang P, Zhu T, Yuan H, Lan J, Yang X, Sui G. *Adv Sci*, 2022, 9: e2103663
45 Zhang Z, Wang J, Zhang S, Ying H, Zhuang Z, Ma F, Huang P, Yang T, Han G, Han WQ. *Energy Storage Mater*, 2021, 43: 229–237
46 Cheng XB, Yang SJ, Liu Z, Guo JX, Jiang FN, Jiang F, Xiong X, Tang WB, Yuan H, Huang JQ, Wu Y, Zhang Q. *Adv Mater*, 2024, 36: 2307370
47 Wu J, Zhou T, Zhong B, Wang Q, Liu W, Zhou H. *ACS Appl Mater Interfaces*, 2022, 14: 27873–27881
48 Dong W, Ye B, Cai M, Bai Y, Xie M, Sun X, Lv Z, Huang F. *ACS Energy Lett*, 2023, 8: 881–888